China Instrument and Control Society
Instrumentation
OPEN ACCESS
INSTRUMENTATION, Vol. 11, No. 4, December 2024 https://doi.org/10.15878/j.instr.202400213

Article

A Partial Differential ANRDPM Image Denoising Model Based on A New Anti-Noise Coefficient and Reverse Diffusion Idea

Yuze Chen[1], Xianchun Zhou[2*], Siqi Lu[1], Binxin Tang[1], Mengnan Lv[1], Zhiting Du[1]

[1] School of Electronic and Information Engineering, Nanjing University of Information Science and Technology, Nanjing 210044, China

[2] School of Artificial Intelligence (School of Future Technology), Nanjing University of Information Science and Technology, Nanjing 210044, China

[*] Corresponding author email: zhouxc2008@163.com

Abstract: To overcome the problem of insufficient expression of fine texture when gradient mode is used as an image feature extraction operator in traditional PM model, which leads to excessive diffusion in these fine texture regions and texture ambiguity, this paper proposes ANRDPM(Anti-noise and Reverse Diffusion PM model) noise reduction model based on the new anti-noise coefficient and reverse diffusion concept. In this model, the meter gradient operator is used as the image feature extractor to solve the shortage of the traditional gradient operator in the ability to express details. Secondly, a new anti-noise coefficient based on Gaussian curvature and noise intensity is proposed to solve the problem that the meter gradient operator is allergic to large noise points. In addition, a reverse diffusion filter based on a local variance of residuals is introduced to enhance the smoothed texture information in the image. Finally, the new model is discretized by a finite difference algorithm, and simulation results show that the proposed ANRDPM model not only performs well in smoothing image noise, but also effectively protects image texture information and structural integrity.

Keywords: image noise reduction; partial differential equation; new anti-noise coefficient; anisotropy; total variation

Citation: Yuze Chen, Xianchun Zhou, Siqi Lu, Binxin Tang, Mengnan Lv, Zhiting Du."A Partial Differential ANRDPM Image Denoising Model Based on A New Anti-Noise Coefficient and Reverse Diffusion Idea." Instrumentation 11, no.4 (December 2024). https://doi.org/10.15878/j.instr.202400213

1 Introduction

With the advent of the information age, the image, as an efficient and convenient information transmission tool, has become one of the indispensable elements in people's lives. By looking at images, people can intuitively understand things, their appearance, location and other details. However, in the process of image acquisition, transmission and use, various internal and external factors may introduce noise, which reduces the quality of the image and makes the details difficult to identify. With the improvement of living standards, people's requirements for image quality are also increasing. Therefore, how to reduce image noise and protect its details at the same time has been the core issue of current image research[1].

The basic idea of the image noise reduction method[2-6] based on Partial Differential Equation (PDE) is to model the image or the geometric evolution of the image to obtain the variational differential equation, and then solve the differential equation to obtain the noise reduction image. The key of image denoising method based on a partial differential equation is to establish a suitable model and construct a suitable partial differential equation. The most representative is the anisotropic PM (Perona Malik, PM) diffusion model[7,8].

In 1990, Perona and Malik[9] applied the heat conduction equation to the nonlinear field and proposed the nonlinear anisotropic diffusion model - PM model, which promoted the study of nonlinear equations. Subsequently, Catte et al[10] proposed the use of a Gaussian filter to preprocess images and established the CLMC (Constrained Least - Mean – Square) model, aiming at the problem that PM model is sensitive to noise. In 2016, Tebini et al[11] proposed a new diffusion function to protect more texture detail features by introducing the Laplacian operator. In 2018, Wang et al[12] proposed a Hybrid model that combines anisotropy and PM models. In 2020, Zhou Xianchun et al[13] proposed an improved PM model based on residual power and a NAPM model coupled with a fourth-order YK model. In 2021, Yin Suya et al[14] introduced the differential curvature operator to extract the YPM(Yin Perona-Malik) model of image edge information. Riya et al[15] proposed a diffusion function with faster convergence. Due to the faster convergence of the diffusion function, large noise points in the image cannot be smoothed. In 2021, Eslahchi et al[16] proposed a MBM model that coupled total variational, PM model and YK model by weight function to protect image texture and suppress the "ladder effect" of images. In the same year, Wen et al[17] proposed to combine BM3D(Block-Matching and 3D Filtering) method with the non-local PM model to protect more texture details. In 2022, Zhang Xinru et al[18] proposed a piecewise diffusion function based on the gradient change of images, but the gradient threshold selection of the new model needs to be improved. In 2022, Meng Dongdong et al[19] used the weight function constructed by 8-neighborhood and implicit curvature to control the proportion of second-order and fourth-order models in image denoising to achieve adaptive adjustment of denoising intensity. In 2023, Li et al[20] proposed a dynamic threshold function, but its noise reduction image is prone to fragment constant phenomenon in a flat region, resulting in "ladder effect". Not only that, some scholars have also made improvements from the perspective of algorithms, considering that the PM model adopts a "cross shape" discrete algorithm, which will lead to blurred image texture. "M Shape" discrete algorithm [21], finite difference algorithm[22], ADMM(Alternating Direction Method of Multipliers, ADMM algorithm [23] and operator split Radial Basis Function (RBF) collocation method[24] are applied to PM models to protect image texture information. In 2018, Zhang et al. introduced FFDNet (Fast and Flexible Denoising Network) [25], which extends its applicability beyond Gaussian noise by incorporating a noise level map as part of the network input, thereby making it suitable for images with varying levels of noise intensity. Nevertheless, it should be acknowledged that FFDNet may not perform optimally when dealing with certain types of noise or images characterized by high levels of noise intensity. In 2019, Zhang et al. presented CBDNet (Cross-Scale Bi-Directional Network)[26], which adopts a more realistic approach by considering Poisson-Gaussian noise along with signal-dependent and ISP-induced noise effects during training using both synthetic and real noisy images to enhance adaptation to real-world scenarios.

Based on this, this paper proposes a partial differential ANRDPM image noise reduction model based on a new anti-noise coefficient and reverse diffusion idea to protect image texture information and smooth noise. Finally, the new model is compared with a variety of mainstream models, and it performs well in both subjective vision and objective evaluation, which verifies the universality and effectiveness of the proposed model.

2 Related Work

PDE image denoising is a very effective method, and the idea based on anisotropic diffusion is applied in modeling. The concept of diffusion is mainly derived from multi-scale descriptions, which can theoretically be regarded as isotropic heat conduction equations. The corresponding equation is expressed as:

$$\frac{\partial u}{\partial t} = div(\nabla u) \tag{1}$$

Where, $u_{\eta\eta}$ is the noise reduction image in the iterative process, $u_{\varsigma\varsigma}$ is the divergence operator, is the gradient operator. Formula (1) can be expanded along the image gradient direction and edge direction, and the expansion formula is as follows:

$$\frac{\partial u}{\partial t} = u_{\eta\eta} + u_{\varsigma\varsigma} \tag{2}$$

Where, $u_{\eta\eta}$ is the second derivative of the image along the gradient direction and $u_{\varsigma\varsigma}$ is the second derivative of the image along the edge direction.

Equation (2) represents the same rate of diffusion along the gradient direction and edge direction in the process of image denoising, so it is called isotropic equation. This equation can reduce noise, but it will blur the edge texture of the image, so it is not applicable. Therefore, the PM model is referenced, and the diffusion equation of the PM model is

$$\frac{\partial u}{\partial t} = div\left(g\left(|\nabla u|\right)\nabla u\right) \tag{3}$$

Where $g(x)$ is the diffusion function, diffusion function generally has two methods:

$$g_1(x) = \frac{1}{1+\left(\frac{x}{k}\right)^2} \tag{4}$$

$$g_2(x) = \exp\left[-\left(\frac{x}{k}\right)^2\right] \tag{5}$$

Where x is the gradient mode of the image pixel, and k is the gradient mode threshold, which determines whether the edge of the image can be preserved. In PM model, gradient mode is a parameter used to determine whether a pixel in an image is in a flat region or an edge region. When a pixel is in an edge region, the difference between the pixel and its adjacent pixels is higher, and it will have a higher gradient mode. When a pixel is located in a flat region, the pixel is closer to its neighboring pixel, and the gradient mode will be lower. In equations (4), it can be found that the diffusion function is a decreasing function that changes with the gradient mode. Therefore, when the gradient mode is higher, the value of the diffusion function is lower, and the image diffusion is slower, which can protect the texture details of the image. When the gradient mode is low, the value of the diffusion function is higher, the image diffusion is faster, and the noise in the flat area of the image can be smoothed.

The discrete expression of the PM model is:

$$u^{n+1} = u^n + dt*\left(g\left(\left|\nabla u_{s,p}^n\right|\right)\nabla u_{s,p}^n\right) \tag{6}$$

Where, $\nabla u_{s,p}^n$is the gradient of pixel point s in the p direction at time n, that is $\nabla u_{s,p}^n = u_p^n - u_s^n$.

3 ANRDPM model of new anisotropic diffusion

This paper proposes a new image denoising model called Anti-noise and Reverse Diffusion PM model (ANRDPM). Firstly, considering that the traditional PM model uses gradient modulus as the texture detection operator, which inadequately expresses image texture details, the traditional gradient operator is replaced with the Rice-cross-shaped gradient operator to compensate for this deficiency, resulting in the new diffusion model 1. Secondly, due to the sensitivity of the Rice-cross-shaped gradient operator to large noisy points, a new anti-noise coefficient based on Gaussian curvature and noise intensity is introduced to enhance the diffusion rate around large noisy points, yielding the new diffusion model 2. Finally, to preserve more texture details in the image, a reverse diffusion filter based on a local variance of residual images in regions where textures are smoothed out is proposed, leading to the final ANRDPM denoising model.

3.1 New diffusion model based on meter gradient operator 1

In the flatter areas of the image, the gradient modulus value of the fine texture is inherently small, and its initial smoothing intensity will be relatively large. With the progress of the iteration, the fine texture is further smoothed, resulting in a smaller gradient modulus value and a greater smoothing intensity, and thus it will be blurred. To protect the fine texture, an image feature operator with a larger value in this area is required. Therefore, in this section, the traditional gradient operator is replaced by the rice-cross-shaped gradient operator as the feature extractor of the image. The rice-cross-shaped gradient operator contains the information of the central pixel and its 8-neighborhood pixels. The expression of the rice-cross-shaped gradient operator is:

$$T_{i,j} = \sqrt{\begin{pmatrix} \frac{1}{2}\left(\left(u_{i,j-1} - u_{i,j}\right)^2 + \left(u_{i,j+1} - u_{i,j}\right)^2\right) \\ + \frac{1}{2}\left(\left(u_{i-1,j} - u_{i,j}\right)^2 + \left(u_{i+1,j} - u_{i,j}\right)^2\right) \\ + \frac{1}{4}\left(\left(u_{i-1,j-1} - u_{i,j}\right)^2 + \left(u_{i+1,j+1} - u_{i,j}\right)^2\right) \\ + \frac{1}{4}\left(\left(u_{i-1,j+1} - u_{i,j}\right)^2 + \left(u_{i+1,j-1} - u_{i,j}\right)^2\right) \end{pmatrix}} \tag{7}$$

Where,$\frac{1}{2}\left(\left(u_{i,j-1} - u_{i,j}\right)^2 + \left(u_{i,j+1} - u_{i,j}\right)^2\right) + \frac{1}{2}\left(\left(u_{i-1,j} - u_{i,j}\right)^2 + \left(u_{i+1,j} - u_{i,j}\right)^2\right)$ represents the change of x and y directions of the image center pixel, combining forward difference and backward difference, so the coefficient of x and y directions is $\frac{1}{2}$. $\frac{1}{4}\left(\left(u_{i-1,j-1} - u_{i,j}\right)^2 + \left(u_{i+1,j+1} - u_{i,j}\right)^2\right) + \frac{1}{4}\left(\left(u_{i-1,j+1} - u_{i,j}\right)^2 + \left(u_{i+1,j-1} - u_{i,j}\right)^2\right)$ represents the change in the two diagonal directions of the center pixel of the image, and since the distance between the pixels is $\frac{1}{\sqrt{2}}$, the coefficient of the diagonal direction is $\frac{1}{4}$.

The Rice-cross-shaped e gradient operator is compared with the traditional gradient module operator to represent the detail features of noise-free images. cameraman images were used for experimental comparison. The comparison results are shown in Figure 1:

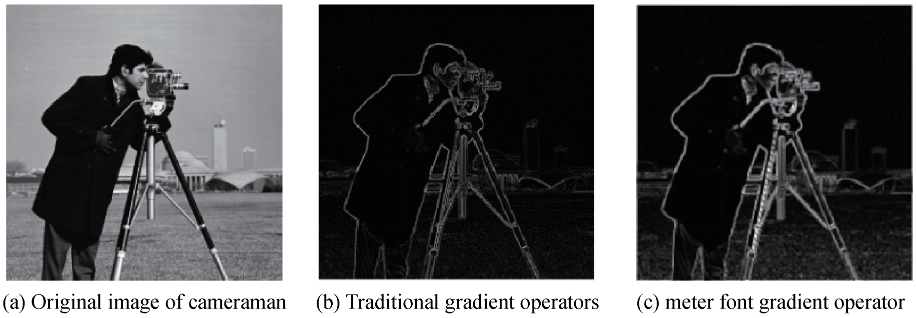

(a) Original image of cameraman (b) Traditional gradient operators (c) meter font gradient operator

Fig.1 Image extraction results of meter font gradient operator and traditional gradient operator

In Figure 1, compared with Figure (b), the edge extraction results of Figure (c) are clearer and the grass texture is richer. Therefore, the Rice-cross-shaped gradient operator has better texture expression ability than the traditional gradient operator.

The meter gradient operator includes not only the gradient values in the x and y directions, but also the gradient values in the diagonal direction, so it can represent more texture details. A new diffusion function is obtained by replacing the gradient module in the PM model with the Rice-cross-shaped operator. The expression is:

$$g(T) = \frac{1}{1+\left(\frac{T}{k_T}\right)^2} \tag{8}$$

Where k_T is the threshold value of the meter type gradient operator. To realize the adaptive threshold value, the average value of the meter type gradient operator $K_T = a*(mean(T))$ is selected as the basis.

3.2 A new diffusion model based on a new anti-noise coefficient 2

Although the meter gradient operator can represent more texture details, it is as susceptible to noise as the traditional gradient operator. If its value is larger at a large noise point, the diffusion function g will have a smaller diffusion value at a large noise point. As the iteration progresses, the model cannot smooth out the large noise points and will retain the large noise points. Figure 2 shows the texture extraction results of the meter type gradient operator of the cameraman image with Gaussian noise.

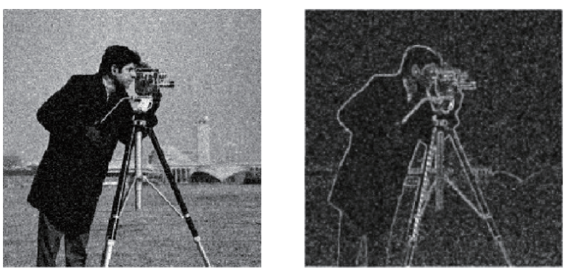

(a) cameraman noise figure (b) The extraction result graph of thegradient operator of rice font

Fig.2 Extraction results of the meter gradient operator of the cameraman noise map

In Figure 2, as shown in Figure (b), at the noise point, the extraction result of the mile-shaped gradient operator is bright, indicating that its value is larger at the noise point, so it will lead to a smaller diffusion value of the diffusion functiong. As the iteration progresses, the model will not be able to smooth out larger noise points. Therefore, it is necessary to distinguish the large noise points from the edge region and the flat region. In this paper, a new anti-noise coefficient based on Gaussian curvature and noise intensity is proposed to enhance the smoothing force of the model at large noise points.

The expression of the Gaussian curvature[25] operator is shown in (9) :

$$G = \left|u_{\eta\eta}\right| * \left|u_{\varsigma\varsigma}\right| \tag{9}$$

Where $u_{\eta\eta}$ is the second derivative of the image along the gradient direction, $u_{\eta\eta} = \dfrac{u_{xx}u_y^2 - 2u_{xy}u_xu_y + u_{yy}u_x^2}{u_x^2+u_y^2}$ and $u_{\varsigma\varsigma}$ is the second derivative of the image along the edge direction, $u_{\varsigma\varsigma} = \dfrac{u_{xx}u_x^2 + 2u_{xy}u_xu_y + u_{yy}u_y^2}{u_x^2+u_y^2}$. u_x, u_y, u_{xx}, u_{yy}, u_{xy} adopt central difference algorithm.

According to formula (9), at the noise point, if $\left|u_{\varsigma\varsigma}\right|$ is larger and $\left|u_{\eta\eta}\right|$ is larger, the value G is larger; In the edge direction of the image, $\left|u_{\varsigma\varsigma}\right|$ is smaller and $\left|u_{\eta\eta}\right|$ is larger, then G is the second. In the flat area of the image, if $\left|u_{\varsigma\varsigma}\right|$ is smaller and $\left|u_{\eta\eta}\right|$ is smaller, the value is smaller. Therefore, the Gaussian curvature G can distinguish the noise points.

The properties of noise points can be distinguished by Gaussian curvature, and a new anti-noise coefficient based on Gaussian curvature and noise intensity is proposed. The expression of the new anti-noise coefficient.

$$AN = 1 - \arctan\left(\sqrt{\sigma_n} * \left(norm(G)\right)^{1.5}\right) \Big/ \left(pi/2\right) \tag{10}$$

Where, $norm$ is the normalization processing, $norm(s) = \dfrac{s - \min\left(s(:)\right)}{\max\left(s(:)\right) - \min\left(s(:)\right)}$, σ_n is the noise intensity of the image in the iteration, using two Laplacian filters for noise reduction, and calculating the noise intensity according to the noise reduction map, the expression is as follows:

$$\sigma_n = \sqrt{\frac{\pi}{2}}\frac{1}{6(M-2)(N-2)}\sum_{imageI}\left|u*L\right| \tag{11}$$

Where (M,N) is the size of the image, u is the noise image, and L is the difference between two different Laplacian filters.

In formula (10), $\sigma_n$is the noise intensity of the image in the iterative process. Two Laplacian filters are used to denoise the noise, and the noise intensity is calculated according to the denoising figure. Therefore, according to the noise intensity of the image, we can judge whether the noise point is a large noise point or a small noise point. After the previous analysis, it is necessary to extract the large noise points. When σ_n is large and $norm(G)$ tends to 1, it represents the large noise point region of the image, and AN tends to 0. Formula (10) indicates that large noise points in the image are distinguished in the iterative process.

A new diffusion function $g(T, AN) = g(T.*AN)$ is obtained by multiplying the anti-noise coefficient $AN$with the meter gradient operator, and a new diffusion model 2 is obtained. The new diffusion model 2 increases the smoothing intensity of the large noise points, while the diffusion intensity of the texture detail regions remains unchanged, thus smoothing out the large noise points.

3.3 A new ANRDPM image noise reduction model based on the idea of anti-noise coefficient and reverse diffusion

Although the new diffusion model 2 increases the smoothing power at large noise points, it still blurs the texture information of the image. To protect more texture details, based on the idea that the residuals have a large variance and reverse diffusion in the smoothing texture region, a new ANRDPM noise reduction model is proposed based on the local variance of residuals.

By decomposing the PM model along the image edge direction and gradient direction, we can get:

$$\frac{\partial u}{\partial t} = div\left(g\left(|\nabla u|\right)\nabla u\right) = g\left(|\nabla u|\right)u_{\varsigma\varsigma} + \frac{1-\left(|\nabla u|/k\right)^2}{\left(1+\left(|\nabla u|/k\right)^2\right)^2}u_{\eta\eta} \tag{12}$$

Where $u_{\eta\eta}$ is the second derivative of the image along the gradient direction; $u_{\varsigma\varsigma}$ is the second derivative of the image along the edge. Figure 3 is a graph of the coefficients of $u_{\eta\eta}$、$u_{\varsigma\varsigma}$ and the image gradient.

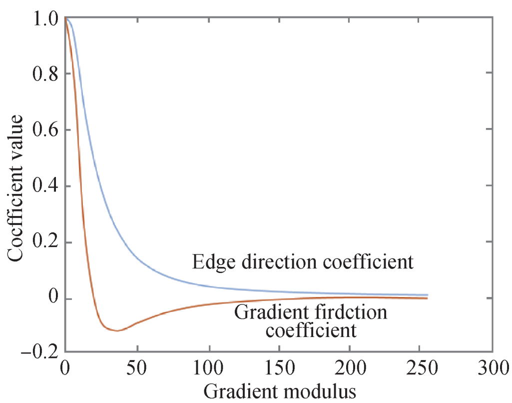

Fig.3 The coefficients of the PM model along the edge and gradient direction vary with the gradient mode

It can be seen from Figure 3 that when the PM model diffuses along the gradient direction, when the gradient value is greater than the threshold value, the diffusion coefficient along the gradient direction is less than 0, that is, reverse diffusion can be carried out to strengthen the texture information.

The PM model has the phenomenon of reverse diffusion along the gradient direction, which can strengthen the edge texture information. In the iterative process of image noise reduction, the partial differential model will not only smooth the noise, but also blur the image texture information. Therefore, the idea of reverse diffusion can be combined with the reverse diffusion in the area of fuzzy texture to strengthen the texture, to protect the details. To distinguish the texture areas that are blurred during iteration, the concept of residual graph can be borrowed. In each iteration, the smoothing force of the PDE is small at the edge of the image, so the edge of the image is roughly retained, while in the fine texture area of the image, the smoothing force of the model is larger, which not only smooths out the noise, but also blurs the texture information. Therefore, in the residual graph, the prescription difference is smaller at the edge of the original image, while the prescription difference is larger in the texture region. When the noise is smoothed off, because the texture of the image is also blurred, the variance of the corresponding area of the texture region is basically greater than the noise variance of the original image. Therefore, to distinguish the area larger than the original image noise variance, with the help of the idea of reverse diffusion, more texture information can be protected. As shown in Figure 4, this is the local variance map of the noise reduction residual results of the PM model.

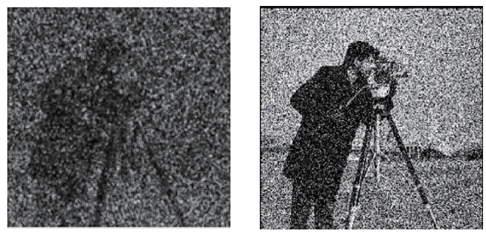

Fig.4 Local variance diagram of the noise reduction residual results from cameraman

In Figure 4, it can be found that the edge of the image is very dark, indicating that the value here is small; the flat area is brighter, indicating that the value is larger. Combined with the previous analysis, the noise intensity of the original image is set as a threshold. When the local variance of the residual map is greater than this threshold, it indicates that the image texture is blurred and the texture needs to be strengthened in reverse. In this paper, a new ANRDPM image noise reduction model based on residual graph and reverse diffusion is proposed. Its expression is as follows:

$$DN = \arctan\left(\sqrt{\sigma_{uc}/\sigma_n}\right)/\left(\pi/2\right) \tag{13}$$

$$\frac{\partial u}{\partial t} = div\left(g\left(T, AN\right)\nabla u\right) - u_{\eta\eta}.*DN*0.7*\frac{1}{1+\left(\frac{T}{K_T}\right)^2} \tag{14}$$

In formula (13), σ_n is the noise intensity of the original image; σ_{uc} is the local standard deviation of the residual graph. In equation (14), $u_{\eta\eta}$ is the second derivative of the image along the gradient direction, and when the coefficient is negative, it represents reverse diffusion.

Formula (13) uses the noise intensity of the original image as the threshold. When the local standard deviation of the residual map is greater than this threshold, $DN \to 1$ distinguishes the blurred image texture region. Formula

(14) indicates that the reverse diffusion is carried out in the distinguished image texture area, and the intensity is$0.7*\frac{1}{1+\left(\frac{T}{K_T}\right)^2}$. Through the previous analysis, in the residual graph, the prescription difference of the image edge is small, indicating that the edge of the image does not change much, so the edge does not need a large reverse diffusion force, while the texture area of the image has a large variance, indicating a large change here, so the texture area needs a large reverse diffusion force.

Therefore, the decreasing function of the reverse diffusion intensity with the change of the Rice-cross-shaped gradient operator is selected. ANRDPM noise reduction model can protect more image texture information by using the idea of reverse diffusion and residual graph.

3.4 Discrete form of the new ANRDPM model

In this paper, the finite difference algorithm is used to discretize ANRDPM model. In order to get the discrete form more easily, the PM model is first discretized by finite difference, and a general expression is obtained. The discretized expression is as follows:

$$\begin{aligned}
\frac{\partial u}{\partial t} &= div\left(g\left(|\nabla u|\right)\nabla u\right) \\
&= \frac{\partial}{\partial x}\left[\left(g\left(|\nabla u|\right)\right)\frac{\partial u}{\partial x}\right]+\frac{\partial}{\partial y}\left[\left(g\left(|\nabla u|\right)\right)\frac{\partial u}{\partial y}\right] \\
&= \frac{\partial}{\partial x}\left[\left(g\left(|\nabla u|\right)\right)\frac{1}{\Delta x}\left(u\left(x+\frac{\Delta x}{2},y,t\right)-u\left(x-\frac{\Delta x}{2},y,t\right)\right)\right] \\
&\quad +\frac{\partial}{\partial y}\left[\left(g\left(|\nabla u|\right)\right)\frac{1}{\Delta y}\left(u\left(x,y+\frac{\Delta y}{2},t\right)-u\left(x,y-\frac{\Delta y}{2},t\right)\right)\right] \\
&= \frac{1}{\Delta x}\left\{g\left(x+\frac{\Delta x}{2},y,t\right)\frac{1}{\Delta x}\left(u\left(x+\Delta x,y,t\right)-u\left(x,y,t\right)\right)\right\} \\
&\quad -\frac{1}{\Delta x}\left\{g\left(x-\frac{\Delta x}{2},y,t\right)\frac{1}{\Delta x}\left(u\left(x,y,t\right)-u\left(x-\Delta x,y,t\right)\right)\right\} \\
&\quad +\frac{1}{\Delta y}\left\{g\left(x,y+\frac{\Delta y}{2},t\right)\frac{1}{\Delta x}\left(u\left(x,y+\Delta y,t\right)-u\left(x,y,t\right)\right)\right\} \\
&\quad -\frac{1}{\Delta y}\left\{g\left(x,y-\frac{\Delta y}{2},t\right)\frac{1}{\Delta x}\left(u\left(x,y,t\right)-u\left(x,y-\Delta y,t\right)\right)\right\}
\end{aligned} \tag{15}$$

Where dt is the time step and $\Delta x=\Delta y=1$ is the space step, then formula (15) can be reduced to:

$$u_{i,j}^{n+1}=u_{i,j}^{n}+dt*\left(\sum_{(a,b)\in\Gamma_{(i,j)}}\left(\left(\frac{g_{a,b}^{n}+g_{i,j}^{n}}{2}\right)\bullet\left(u_{a,b}^{n}-u_{i,j}^{n}\right)\right)\right) \tag{16}$$

Wherein, the pixel coordinate (a,b) is located in the cross-shaped neighborhood of the pixel coordinate (i,j).

The discrete form of the ANRDPM model can be obtained by substituting the diffusion function into equation (16).

3.5 Noise reduction process of the new ANRDPM model

Table 1 Noise reduction process of ANRDPM model

Import noise image, time interval dt, iteration number N
1. Calculate the meter gradient operator, Gaussian curvature, anti-noise coefficient and reverse filter coefficient of the image, and substitute them into the discrete form of the new ANRDPM model.
2. According to the number of iterations, obtain the PSNR value of the noise reduction image for each iteration.
3. Output the noise reduction image corresponding to the best PSNR value, and calculate the corresponding SSIM value.

4 Experimental results and analysis

4. 1 Experiment and parameter setting

This section mainly conducts experimental verification and analysis of the proposed ANRDPM model based on anisotropic diffusion. The processor used in the experiment is Intel(R) Core(TM) i5-8265U CPU @ 1.60 GHz 1.80 GHz, GPU NVIDIA GeForce RTX 3090 and the memory is 8.0 GB. The operating system is Windows10 64-bit; The running environment is MATLAB R2017b.

To verify the validity of this model, Four standard images (cameraman(256×256), peppers(256×256), man (512×512) and ship (512×512)) and four captured images (lion) were selected from image dataset Set12 (256×256), flowers(256×256), city (512×512), and lake(512×512). Among them, images such as cameraman are relatively flat, which can be used to verify the noise reduction capability of the model. Images such as city and man have rich textures, so they can be used to verify the model's ability to protect textures. Peppers et al., with clear edges, can be used to verify the model's edge retention ability. Different degrees of Gaussian noise were added for simulation experiments. The original image required for the experiment is shown in Figure 5.

In order to verify the effectiveness of the new ANRDPM model, PM model, CLMC model, YK model, NAPM model [17], and YPM model [12], FFDNet and CBDNet were used for noise reduction experiments to prove the ability of the new ANRDPM model to reduce noise and preserve edges. The reasons for choosing these comparison algorithms are as follows:

(1) PM model is the classical anisotropic diffusion model in the field of partial differential equations, and the new model is improved on this basis, so the PM model is used as a contrast model;

(2) CLMC model is a regularized PM model proposed by Catte et al., which solves the problem that PM model is sensitive to noise;

(3) YK model is a high-order diffusion model in the field of partial differential equations, which solves the

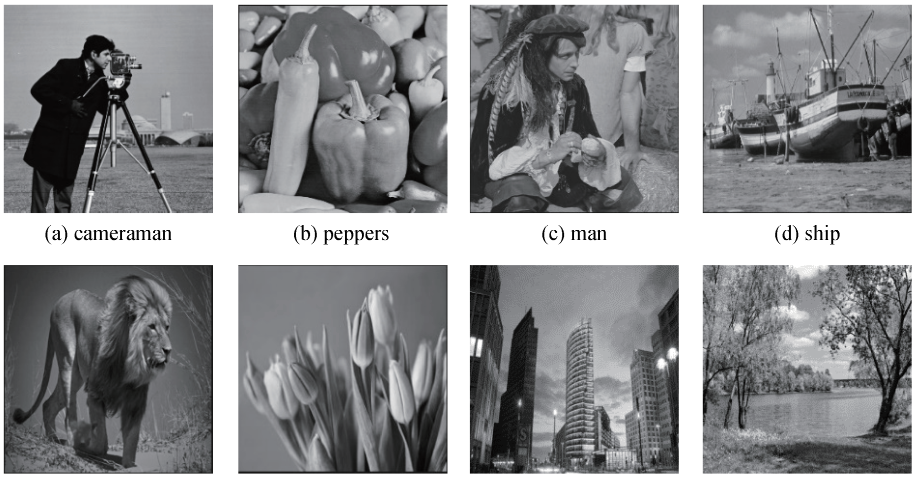

(a) cameraman (b) peppers (c) man (d) ship

(e) lion (f) flowers (g) city (h) lake

Fig.5 cameraman and other eight original images

"ladder effect" problem of PM model;

(4) NAPM model is an improved PM model proposed in literature[17]. When the residual power meets certain conditions, the residual power is introduced into the diffusion function to protect the image texture together with the gradient model;

(5) YPM model is an improved model proposed in literature[12]. Differential curvature operators are introduced into PM model to extract image edge information, and the properties of fractional differential operators are combined to enhance the smoothing in flat regions.

It is also compared with FFDNet and CBDNet to verify the superiority of corresponding innovation points.

4.2 Comparison experiment of noise reduction index values of new ANRDPM model

ANRDPM model, PM model, CLMC model (C model), YK model, NAPM model, YPM model, FFDNet and CBDNet were used to reduce noise, and the ability of ANRDPM model to reduce noise and preserve edges was proved.

Set the parameters of the model$dt = 0.02$, make the time step of the partial differential model, set the parameters of the PM model, the C model and the YK model to be the same, and set the gradient threshold to 20. The optimal PSNR and SSIM values of each model are obtained.

Table 2 shows the PSNR values of images after noise reduction of various models, and the best values are bolded. Table 3 shows the SSIM values of images after noise reduction of various models, and the best values are bolded.

When comparing and analyzing the results in Tables 1, 2, and 3, the newly proposed ANRDPM model shows significant advantages in terms of peak signal-to-noise ratio (PSNR) values and structural similarity (SSIM) values. The following is a detailed evaluation and analysis of these metrics: In Table 1, the average PSNR values between the models clearly show the performance of the different models in the image reconstruction task. In particular, as a high-order diffusion model, the "ladder effect" of YK model is somewhat suppressed, but it leads to the blurring of image texture, so that the average PSNR value of YK model is the lowest. Although PM model has improved this problem, its performance is still not up to the best state. C model, NAPM model and YPM model are all improvements of PM model, and their average PSNR values are higher than those of PM model, indicating that these improvements can improve image quality. In particular, the average PSNR value of the new ANRDPM model was significantly higher than that of the PM model in all test images, showing a significant advantage in peak-to-noise ratio. This shows that the ANRDPM model can recover image details more efficiently and reduce noise, thus providing higher quality image reconstruction results. In addition, the introduction of FFD model and CBD model further proves the advantages of ANRDPM model. FFD model can improve PSNR value to some extent by introducing additional feature mapping and multi-scale fusion. In contrast, the new ANRDPM model can better combine the global and local information of the image, ensuring consistency and efficiency at different noise levels. CBD model also provides good performance in image denoising, but ANRDPM model's improvement in overall performance makes it more advantageous in terms of peak signal-to-noise ratio. In Table 2 and Table 3, SSIM value, as an important index to measure the similarity of image structure, also indicates the superiority of ANRDPM model. Compared with the traditional PM model and its improved version, ANRDPM model not only performs well in PSNR value, but also shows higher image structure retention ability in SSIM value. ANRDPM model can effectively retain the structure information of the image while improving the detail recovery of the image, so that the reconstructed image can perform better in terms of visual quality and structural similarity. Taking

Table 2 PSNR(dB) values of ANRDPM comparison model after noise reduction

σ_n	Image	PM	C	YK	NAPM	YPM	FFDNet	CBDNet	ANRDPM
10	cameraman	32.670	32.418	31.497	32.697	32.808	33.102	33.109	**33.138**
	peppers	33.613	33.457	32.208	33.675	33.719	33.986	33.103	**33.988**
	man	32.925	32.877	31.948	32.981	33.014	33.155	**33.180**	33.176
	ship	32.634	32.682	31.678	32.685	32.714	32.760	32.771	**32.773**
	lion	32.232	32.172	31.330	32.241	32.322	32.665	32.640	**32.671**
	flowers	34.060	34.133	32.700	34.252	34.322	34.363	34.405	**34.523**
	city	32.679	32.529	31.486	32.728	32.922	**33.210**	33.163	33.202
	lake	29.857	29.915	29.281	29.857	30.017	30.099	**30.110**	30.107
20	cameraman	28.805	28.791	27.081	28.935	29.141	29.330	29.320	**29.361**
	peppers	29.906	29.990	27.952	29.975	30.099	30.274	30.280	**30.296**
	man	29.582	29.690	28.356	29.730	29.752	29.723	29.833	**29.836**
	ship	29.264	29.459	28.045	29.416	29.542	29.503	29.498	**29.546**
	lion	28.794	28.907	27.669	28.953	28.954	29.140	29.180	**29.194**
	flowers	30.278	30.584	28.493	30.509	30.669	**30.780**	30.754	30.756
	city	28.594	28.741	27.268	28.806	28.964	29.320	**29.405**	29.212
	lake	25.470	25.736	24.626	25.470	25.747	25.850	25.864	**25.866**
30	cameraman	26.483	26.580	24.674	26.571	26.869	27.012	26.967	**27.110**
	peppers	27.826	28.050	25.771	27.873	28.088	**28.352**	28.237	**28.337**
	man	27.701	27.930	26.567	27.893	27.921	27.705	**28.210**	28.177
	ship	27.349	27.684	26.225	27.579	27.706	**28.105**	27.914	27.959
	lion	27.015	27.231	26.010	27.195	27.207	27.384	27.488	**27.493**
	flowers	27.930	28.432	26.301	28.206	28.390	28.620	28.652	**28.675**
	city	26.418	26.724	25.345	26.660	26.834	27.163	27.106	**27.170**
	lake	23.287	23.655	22.572	23.438	23.593	23.524	23.811	**23.822**
40	cameraman	24.873	25.073	23.154	24.915	25.327	25.650	25.758	**25.772**
	peppers	26.262	26.648	24.439	26.382	26.562	26.882	26.875	**26.901**

Continue Table 2 PSNR(dB) values of ANRDPM comparison model after noise reduction

σ_n	Image	PM	C	YK	NAPM	YPM	FFDNet	CBDNet	ANRDPM
40	man	26.447	26.765	25.498	26.668	26.700	27.001	26.971	**27.018**
	ship	25.921	26.342	24.941	26.208	26.296	26.528	26.630	**26.664**
	lion	25.780	26.118	25.042	25.972	26.014	**26.450**	26.358	26.429
	flowers	26.391	27.016	24.941	26.724	26.883	27.306	27.258	**27.318**
	city	24.852	25.287	24.068	25.158	25.271	25.535	**25.735**	**25.725**
	lake	21.948	22.366	21.394	22.205	22.230	22.499	22.532	**22.535**
Mean value		28.370	28.562	27.143	28.517	28.644	28.587	28.828	**28.898**

PSNR and SSIM into consideration, the new ANRDPM model shows significant advantages in image denoising and reconstruction tasks. Although the average PSNR value of the C model is higher than that of the PM model, its performance is not as stable as that of the ANRDPM model under specific noise levels, especially when the noise standard deviation is 10, the performance of the C model decreases significantly. While FFD and CBD

Table 3 SSIM values of ANRDPM comparison model after noise reduction

σ_n	Image	PM	C	YK	NAPM	YPM	FFDNet	CBDNet	ANRDPM
10	cameraman	0.873	0.857	0.856	0.890	0.874	0.904	0.903	**0.905**
	peppers	0.908	0.901	0.889	0.912	0.907	0.919	0.920	**0.921**
	man	0.950	0.948	0.944	0.952	0.950	0.953	0.954	**0.957**
	ship	0.949	0.947	0.941	0.952	0.949	0.952	0.955	**0.956**
	lion	0.872	0.865	0.856	0.881	0.871	**0.898**	0.895	0.897
	flowers	0.923	0.919	0.909	0.940	0.924	0.948	0.951	**0.952**
	city	0.946	0.941	0.935	0.954	0.947	0.962	**0.965**	0.963
	lake	0.966	0.965	0.962	0.966	0.966	0.966	0.967	**0.969**
20	cameraman	0.795	0.780	0.756	0.814	0.804	0.839	0.840	**0.841**
	peppers	0.851	0.843	0.815	0.854	0.852	0.872	**0.874**	**0.874**
	man	0.890	0.887	0.876	0.897	0.890	0.899	0.900	**0.901**
	ship	0.886	0.883	0.871	0.894	0.887	0.901	0.900	**0.902**
	lion	0.775	0.770	0.752	0.791	0.778	0.801	0.803	**0.805**
	flowers	0.866	0.863	0.833	0.888	0.869	0.904	0.905	**0.906**
	city	0.881	0.869	0.858	0.897	0.882	0.911	0.912	**0.915**
	lake	0.906	0.905	0.894	0.906	0.909	0.912	0.913	**0.914**
30	cameraman	0.739	0.719	0.689	0.747	0.748	0.785	0.785	**0.787**
	peppers	0.806	0.800	0.763	0.804	0.807	0.830	0.832	**0.834**
	man	0.837	0.835	0.819	0.844	0.838	0.850	0.852	**0.853**

Continue Table 3 SSIM values of ANRDPM comparison model after noise reduction

σ_n	Image	PM	C	YK	NAPM	YPM	FFDNet	CBDNet	ANRDPM
30	ship	0.833	0.828	0.811	0.840	0.835	0.854	0.855	**0.857**
	lion	0.704	0.707	0.680	0.721	0.711	0.735	0.736	**0.737**
	flowers	0.811	0.813	0.775	0.832	0.819	0.860	0.862	**0.864**
	city	0.826	0.809	0.797	0.839	0.826	0.859	0.864	**0.865**
	lake	0.844	0.846	0.827	0.847	0.849	0.854	0.853	**0.856**
40	cameraman	0.696	0.679	0.641	0.692	0.709	0.750	0.757	**0.758**
	peppers	0.764	0.765	0.730	0.764	0.772	0.799	0.803	**0.806**
	man	0.791	0.792	0.772	0.799	0.795	0.805	0.809	**0.812**
	ship	0.783	0.782	0.759	0.792	0.787	0.809	0.811	**0.814**
	lion	0.653	0.661	0.640	0.671	0.663	0.690	**0.692**	**0.692**
	flowers	0.758	0.769	0.728	0.784	0.774	0.819	0.822	**0.823**
	city	0.776	0.762	0.743	0.785	0.781	**0.825**	0.820	0.821
	lake	0.780	0.789	0.765	0.787	0.788	0.797	0.798	**0.799**
Mean value		0.832	0.828	0.809	0.842	0.836	0.858	0.859	**0.861**

models offer different improvement strategies, the ANRDPM model, with its innovative reverse filter and optimization algorithm, can achieve higher PSNR and SSIM values under a variety of noise conditions, thus surpassing these traditional models in overall performance. Therefore, the new ANRDPM model not only performs best in terms of peak signal-to-noise ratio and structural similarity, but also shows obvious advantages in stability and image quality improvement under different noise conditions.

4.3 Ablation experiment

To evaluate the necessity of each module in the new ANRDPM model, we conducted a series of ablation experiments: (1) Replacing the ANRDPM Rice-cross-shaped gradient operator with a traditional gradient operator. (2) Remove Gaussian curvature from ANRDPM. (3) Remove the reverse diffusion filter based on the local variance of the residual graph. (4) Fully implement ANRDPM. To ensure the accuracy of the experiment, the models were evaluated on dataset Set12, which consisted of 4 standard images and 4 captured images respectively. The average value of the experiment was selected as the experimental result. The experimental results are shown in Table 4. ANRDPMA contains only Gaussian curvature and reverse diffusion filters. ANRDPMB includes the Rice-cross-shaped gradient operator and Gaussian curvature. ANRDPMC includes a Rice-cross-shaped gradient operator and an inverse filter.

As shown in Table 4, it is clear that the full ANRDPM model is significantly better than the two alternative models, indicating that each module contributes to improved noise reduction performance. The results show that when σ =10, compared with ANRDP and the other three models (ANRDPMA, ANRDPMB, ANRDPMC), the PSNR value is increased by 1.43, 0.14 and 0.19 respectively. When σ =20, the increase is 1.76, 0.06 and 0.18 respectively. When σ=30, the improvements are 1.91, 0.13, and 0.19 respectively, and when σ =50, the improvements are 1.86, 0.11, and 0.20. It is proved that the overall denoising performance can be improved by the combination of the Rice-cross-shaped gradient operator and Gaussian curvature and the inverse filter.

Tab.4 Average PSNR of ablation experiment

σ	10	20	30	40
ANRDPMA	31.51	27.48	25.43	24.18
ANRDPMB	32.80	29.18	27.21	25.93
ANRDPMC	32.75	29.06	27.15	25.84
ANRDPM	32.94	29.24	27.34	26.04

4.4 Network complexity analysis

Table 5 shows a comparison of processing times for different noise reduction algorithms on the Set12 dataset. The experiment involved processing eight images from the Set12 dataset and calculating the average processing time as the final result. It is obvious from the table that ANRDPM model is inferior to other denoising algorithms in terms of image processing time. The new ANRDPM model is suitable for low noise reduction.

Tab. 5 Comparison of average runtime

Methods	PM	C	YK	NAPM	YPM	ANRDPM
Time/s	28.370	28.562	27.143	28.517	28.644	28.898

4.5 Comparison of noise reduction images with the new ANRDPM model

In this section, images cameraman, peppers, and ship in Figure 5 are selected for noise reduction. Among them, the cameraman image smoothing can be used to verify the noise reduction capability of the model. Ship image is rich in texture, which can be used to verify the model's ability to protect texture. Peppers images have clear edges, which can be used to verify the model's edge retention ability. From the subjective point of view, the texture and noise reduction of the noise reduction image are observed to judge the noise reduction effect of each model. Figure 6, Figure 8 and Figure 10 respectively show the noise reduction results of different models with $\sigma = 20, 30, 40$ Gaussian noise, Figure 7, Figure 9 and

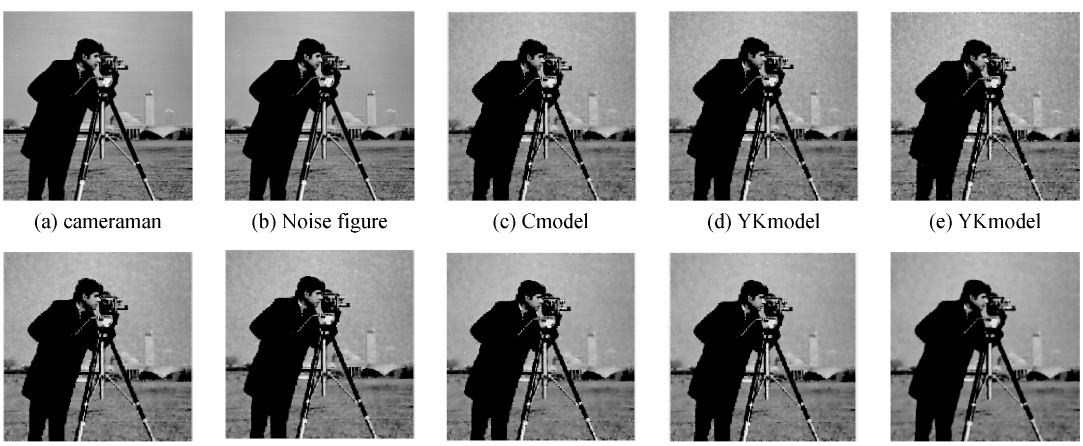

(a) cameraman (b) Noise figure (c) Cmodel (d) YKmodel (e) YKmodel

(f) NAPMmodel (g) YPMmodel (h) FFDNet (i) CBDNet (j) New ANRDPM model

Fig.6 Results of noise reduction by cameraman ($\sigma = 20$), (a) original image, (b) noise image, (c)-(j) results of noise reduction by different models

Figure 11 respectively show the local details of the noise reduction results.

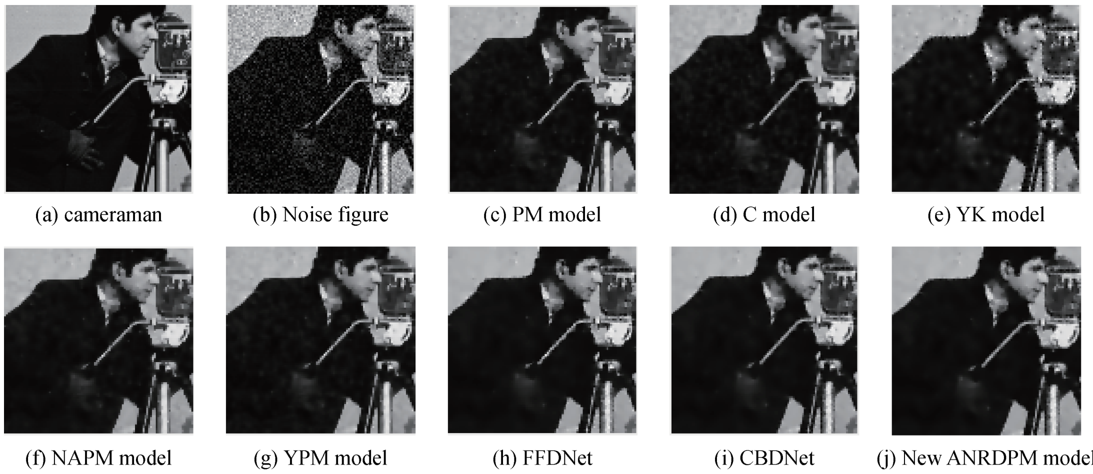

(a) cameraman (b) Noise figure (c) PM model (d) C model (e) YK model

(f) NAPM model (g) YPM model (h) FFDNet (i) CBDNet (j) New ANRDPM model

Fig.7 Local details of cameraman ($\sigma=20$), (a) original image, (b) noise image, (c)-(j) local details of different models

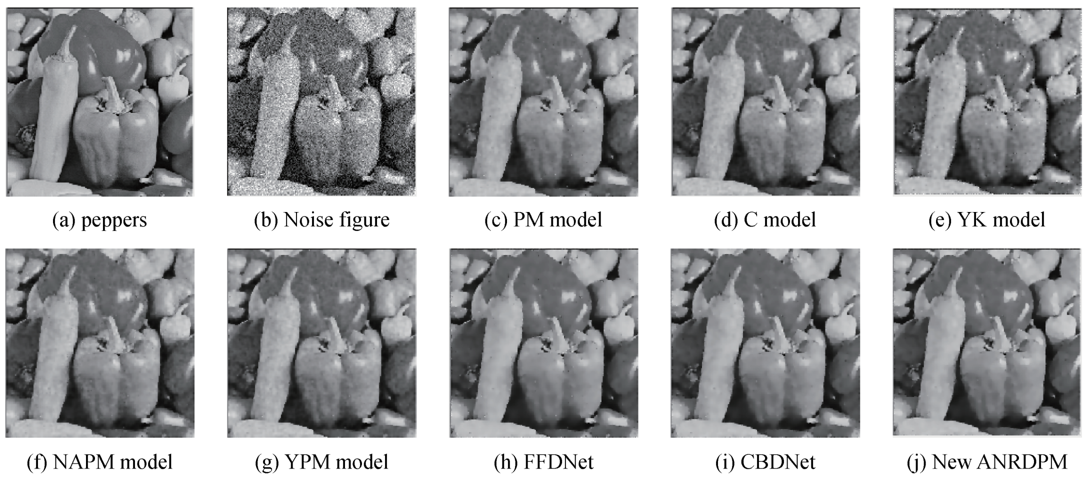

(a) peppers (b) Noise figure (c) PM model (d) C model (e) YK model

(f) NAPM model (g) YPM model (h) FFDNet (i) CBDNet (j) New ANRDPM

Fig.8 peppers Noise reduction results ($\sigma=30$), (a) original image, (b) noise image, (c)-(j) Noise reduction results of different models

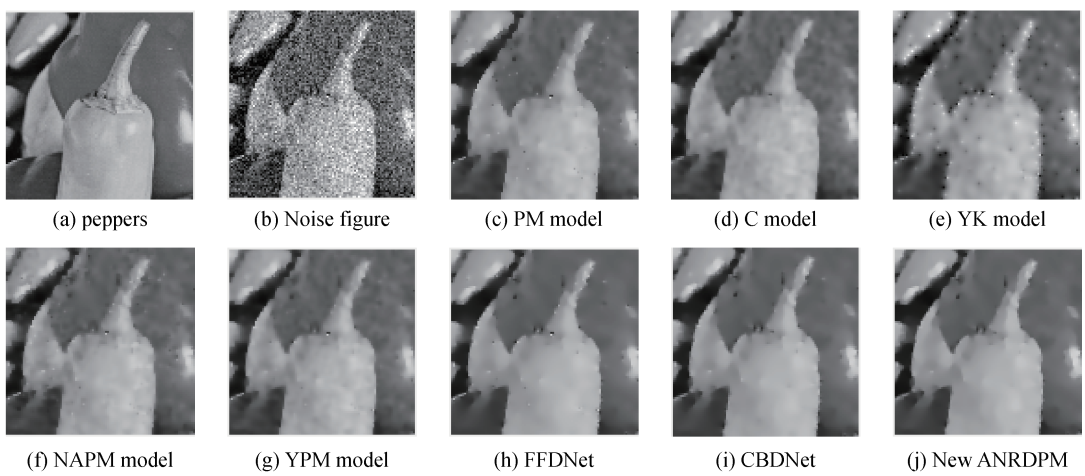

(a) peppers (b) Noise figure (c) PM model (d) C model (e) YK model

(f) NAPM model (g) YPM model (h) FFDNet (i) CBDNet (j) New ANRDPM

Fig.9 peppers Local detail maps ($\sigma=30$), (a) original map, (b) noise map, (c)-(j) Local detail maps of different models

Observe the noise reduction results and local details in Figures 6 through 11. As can be seen from the figure, the noise reduction result graphs of PM model and C model also increase significantly with the increase of noise intensity, and the corresponding local detail graphs are fuzzy and the information is seriously lost. For example, the local details of peppers are obviously fuzzy in the Peppers detail graph, and the sky noise is obvious in the ship detail graph. The YK model uses the Laplace operator as the texture detector of the image, which is sensitive to noise points and will leave black and white noise points. The local detail diagrams in Figure 7(e),

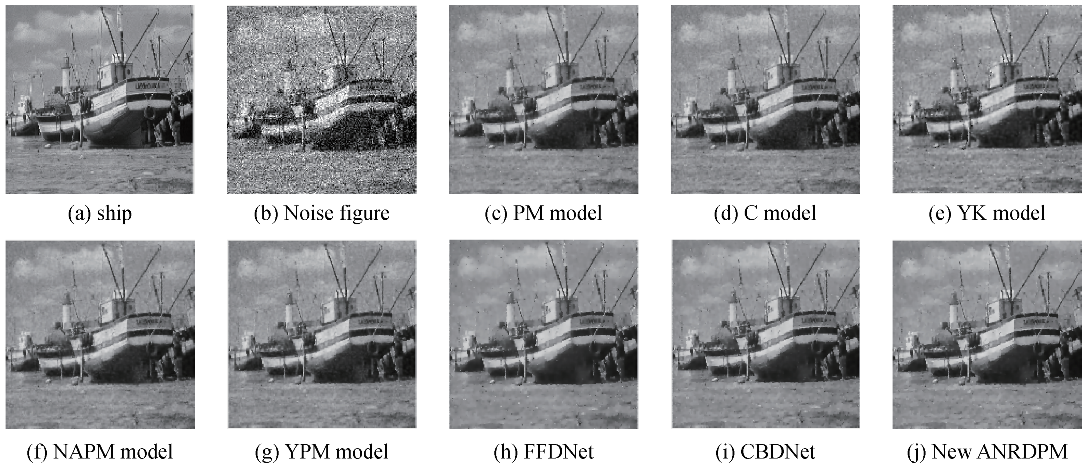

Fig.10 ship noise reduction results ($\sigma = 40$), (a) original image, (b) noise image, (c)-(j) noise reduction results of different models

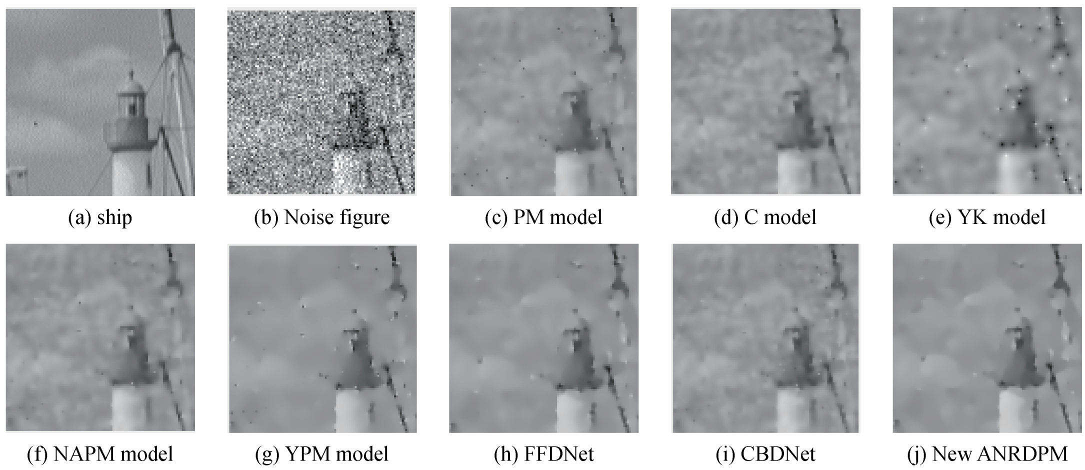

Fig.11 Local detail diagram of ship ($\sigma = 40$), (a) original diagram, (b) noise diagram, (c)-(j) local detail diagram of different models

Figure 9(e) and Figure 11(e) can see obvious black and white noise points. There is obvious noise in the local detail diagram of NAPM model and YPM model, especially in the local detail diagram of ship, which shows that these two models have poor effects in noise reduction with high noise. New diffusion model 1, new diffusion model 2 and new ANRDPM model are the three models proposed in this paper. The new diffusion model 1 uses the meter gradient operator as the image texture detector. On this basis, the new diffusion model 2 uses the anti-noise coefficient to reduce the influence of large noise points, which is conducive to image noise reduction. The new ANRDPM model is based on the new diffusion model 2, and a reverse diffuser based on a residual graph is added to protect more texture details of the image. By observing their corresponding denoising maps, the denoising results showed fewer noise points and clearer images, and the corresponding local enlarged maps had smooth contours. In the peppers overall denoising chart, these three new models were obviously clearer than other models with fewer noise points, and it was also evident that they had fewer noise points in the ship local detail chart. Compared with new diffusion model 1 and new diffusion model 2, the result of new diffusion model 2 in the ship local detail diagram has less black spots than new model 1 when noise reduction is high, which can prove that new diffusion model 2 has stronger noise reduction ability than new diffusion model 1. Compared with the new ANRDPM model and the new diffusion model 2, there is no obvious change to the naked eye, but combined with the noise reduction data PSNR and SSIM in Table 1 and Table 2, the data of the new ANRDPM model is better and more conducive to practical application. In general, according to Table 1, Table 2 and Figure 6 to Figure 11, the new ANRDPM model can obtain better visual effect in terms of the ability of noise reduction and edge preservation, and is more in line with practical application.

5 Conclusion

In this paper, a partial differential ANRDPM image denoising model based on a new anti-noise coefficient and reverse diffusion idea is proposed. Considering that the traditional PM model uses gradient mode as texture detection operator to express the image texture detail is insufficient, the traditional gradient operator is replaced by the Rice-cross-shaped gradient operator to make up for the shortage. Since the Rice-cross-shaped gradient operator is sensitive to large noise points, a new anti-noise coefficient based on Gaussian curvature and noise intensity is established to increase the diffusion rate of the model at large noise points. Finally, in order to protect more image texture details, based on the idea of residual graph and reverse diffusion, a reverse diffusion filter based on local variance of residual graph is proposed, and the final ANRDPM noise reduction model is obtained. The finite difference algorithm is used to get the discrete form of the new model. In the experimental comparison part, the superiority of the new model is proved from the aspects of noise reduction index PSNR and SSIM and subjective noise reduction map, which can balance the noise reduction process and the intensity of texture protection. In terms of running Time, it can be concluded that the new ANRDPM model is suitable for low noise denoise. At the same time, the new ANRDPM model is also suitable for high noise denoise if the time requirement is not strict.

Author Contribution:

Yuze Chen: As the first author, conceived the research idea and designed the overall framework. Conducted in-depth literature review and formulated research questions. Collected and analyzed the majority of the data. Wrote the main body of the manuscript and led the revision process. Xianchun Zhou: Provided guidance on research direction and methodology. Reviewed and critiqued the research design and manuscript at different stages. Siqi Lu: Assisted in data collection and organization. Performed preliminary data analysis and contributed to data interpretation. Binxin Tang: Participated in discussions on research findings and provided valuable feedback for manuscript improvement. Mengnan Lv: Conducted supplementary experiments and validations. Helped in creating visualizations of data and enhancing the presentation of results. Zhiting Du: Supplementary experiments and validations have been conducted. Moreover, assistance has been provided in the creation of data visualizations and the enhancement of result presentations.

Foundation Information:

This research was funded by National Nature Science Foundation of China, grant number 61302188.

Data Availability:

The authors declare that the main data supporting the findings of this study are available within the paper and its Supplementary Information files.

Conflicts of Interest:

The authors declare no competing interests.

Dates:

Received 18 July 2024; Accepted 20 October 2024; Published online 31 December 2024

References

[1] Hadri A , Laghrib A , Mourabit I E .A new learning space-variant anisotropic constrained-PDE for image denoising[J]. *Applied mathematical modelling* , **2024**(Pt.B):125.

[2] Ashouri F, Eslahchi MR. A new PDE learning model for image denoising[J]. *Neural Computing & Applications* , **2022**, 34(11): 8551-8574.

[3] Afraites L, Hadri A, Laghrib A, et al. A weighted parameter identification PDE-constrained optimization for inverse image denoising problem[J]. *The Visual Computer* , **2021**, 38 (8): 2883-2898.

[4] Wen Y, Sun JB, Guo ZC. A new anisotropic fourth-order diffusion equation model based on image features for image denoising[J]. *Inverse Problems and Imaging* , **2022**, 16(4): 895-924.

[5] ZHAO Qingmeng, Wang Pengfei, Xu Xia. Second order PDE denoising Model based on gradient regularization and adaptive reliability [J]. *Information and Computer (Theoretical Edition)* ,**2022**,34(19): 192-194.

[6] Hakoume, A. El, L. Afraites, and A. Laghrib. "*Well-posedness and simulation results of a coupled denoising PDE.* " Nonlinear Analysis: Real World Applications 65(**2022**): 103499-.

[7] Li Q, Hub Y, Cao Y. Adaptive Perona-Malik model based on dynamical threshold for image multi-noise removal with details preservation[J]. *Computers & Mathematics with Applications* , **2023**, 137: 28-43.

[8] Xu Yansong, Zhang Aijun, Yang Meng. Adaptive anisotropic diffusion based on local gradient statistics [J]. *Laser Journal* , **2023**,44(08): 60-64.

[9] Perona P, Malik J. Scale space and edge detection using anisotropic diffusion[J]. *IEEE Transactions on Pattern Analysis and Machine Intelligence* , **1990**, 12: 629-639.

[10] Catté F, Lions P L, Morel J M, et al. Image Selective Smoothing and Edge Detection by Nonlinear Diffusion[J]. *Siam Journal on Numerical Analysis* , **1992**, 29(1): 182-193.

[11] Tebini S, Mbarki Z, Seddik H, et al. Rapid and efficient image restoration technique based on new adaptive anisotropic diffusion function[J]. *Digital Signal Process* , **2016**, 48: 201-215.

[12] Na W, Shang Y, Yang C, et al. A Hybrid Model for Image Denoising Combining Modified Isotropic Diffusion Model and Modified Perona-Malik Model[J]. *IEEE Access* , **2018**, 6: 33568-33582.

[13] Zhou Xianchun, Wang Rong, Wu Jing, et al. Image denoising algorithm based on NAPM mixed fourth-order YK[J]. *Modern Electronic Technology* , **2020**,43(15): 37-41.

[14] Yin Suya, Tang Quan. Adaptive image denoising model based on Partial differential equation [J]. *Bulletin of Science and Technology* ,**2021**, 37(04): 83-87.

[15] Riya, Gupta B, Lamba S S. An efficient anisotropic diffusion model for image denoising with edge[J]. *Computers & Mathematics with Applications* , **2021**, 93(4): 106-119.

[16] Eslahchi MR, Esmaili S, Namaki N, et al. Application of finite difference method in solving a second- and fourth-order PDE blending denoising model[J]. *Mathematical Sciences* , **2021**, 17(1): 93-106.

[17] Wen Y, Guo ZC, Yao WJ, et al. Hybrid BM3D and PDE Filtering for Non-Parametric Single Image Denoising[J]. *Signal Processing* , **2021**(184): 108049.

[18] Zhang Xinru, Zhou Xianchun, Wang Zhifeiet al. Image denoising algorithm based on improved anisotropic diffusion [J]. *Electronic Measurement Technology* ,**2022**,45(17): 113-119.

[19] Li Q, Hub Y, Cao Y. Adaptive Perona-Malik model based on dynamical threshold for image multi-noise removal with details preservation[J]. *Computers & Mathematics with Applications* , **2023**, 137: 28-43.

[20] Meng Dongdong, Zhou Xianchun, Wang Wenyanet al. Multi-order Partial differential Equation hybrid denoising based on 8-neighborhood and curvature[J]. *Computer and Digital Engineering* ,**2022**,50(09):2089-2092+2125.

[21] Zhai Donghai, Yu Jiang, Duan Weixiaet al. Image denoising algorithm of Metre-shaped anisotropic diffusion model[J]. *Computer Applications* , **2014**,34(05): 1494-1498.

[22] Eslahchi MR, Esmaili S, Namaki N, et al. Application of finite difference method in solving a second- and fourth-order PDE blending denoising model[J]. *Mathematical Sciences* , **2021**, 17(1): 93-106.

[23] Sniba F, Karami F, Meskine D. ADMM algorithm for some regularized Perona-Malik equation and applications to image denoising[J]. *Signal Image and Video Processing* , **2023**, 17 (3): 609-617.

[24] Lotfi Y, Parand K. Efficient image denoising technique using the meshless method: Investigation of operator splitting RBF collocation method for two anisotropic diffusion-based PDEs [J]. *Computers & Mathematics with Applications* , **2022**, 113: 315-331.

[25] Zhang K, Zuo W, Zhang L, FFDNet: Toward a fast and flexible solution for cnn-based image denoising, [J]. *IEEE Trans on Image Processing* ,**2018**,27 (9):4608-4622.

[26] Guo S, Yan Z F, Zhang K, et al. Toward convolutional blind denoising of real photographs[C]//Proceedings of the IEEE/ CVF Conference on Computer Vision and Pattern Recognition, Jun. 16-20, 2019, Long Beach, USA. IEEE Press, **2019**:1712-1722.